Synthetic Ionophores. 13. Pyridine−Diamide−Diester Receptors: Remarkable Effect of Amide Substituents on Molecular Organization and Ag^+ Selectivity

Subodh Kumar,* Maninder Singh Hundal, Navneet Kaur, Rajinder Singh, and Harjit Singh*

Department of Chemistry, Guru Nanak Dev University, Amritsar-143 005, India

Geeta Hundal nee Sood, Martin Martinez Ripoll, and Juliana Sanz Aparicio

Departmento de Cristalografia, Instituto de Quimica Fisica, Rocasolano, Serrano-119, E-28006, Madrid, Spain

Received May 9, 1996[⊗]

The $N_{Py}\cdots HN_{amide}$ hydrogen bonding within the macrocyclic cavities in **9**, **10**, and **13** invokes their symmetrical electron-deficient structures (^{1}H NMR) and consequently bind with water. This results in their poor ionophore characters. The steric requirement of methyl/benzyl substituents on amide N in **11** and **12** takes the substituents out of the cavity and thus positions the amide O toward the cavity (^{1}H, ^{13}C NMR and X-ray analysis). This arrangement of two pyridine N and two amide O (^{13}C NMR, IR) binding sites provides an appropriate environment for selective binding toward Ag^+ over Pb^{2+}, Tl^+, alkali, and alkaline earth cations. The increased spacer length in **14** leads to a lop-sided twist of pyridine rings (X-ray) and disturbs the above arrangement and leads to its poor binding character.

Introduction

A rational design of macromolecular receptors is governed by a number of factors (the nature, the number, the relative structural and spatial placement of various ligating units, etc.), and the combination of these factors induces an intrinsic balance of noncovalent binding forces optimum for specificity in host−guest recognition.[1] The amide group, so generously used by nature in a variety of antibiotic ionophores,[2] etc., has acquired a special status in the design of receptors because it displays dual (O or N and NH) ligating character, higher negative charge on oxygen than ether and ester groups, and geometrical rigidity.[3] Pyridine−amide-based macrocycles for selective recognition of metal cations[4] and organic molecules[5] adopt preorganization of their binding sites through hydrogen bonding or configurational rigidity around the amide carbon−nitrogen bond. Among pyridine-based macrocycles, the binding trends of pyridine−amines,[6] pyridine−ethers/pyridine−amide/thioamide−ethers,[7] pyridine ether−ester[8] have been studied toward transition metal ions, amines/ammonium cations, and alkali, alkaline earth cations, respectively. The 18-membered pyridine−ether−ester macrocycles have exhibited slightly better binding for Ag^+ against even alkali metal cations. This preference is further increased in a pyridine−thioether−ether macrocycle.[9] Here, we report our findings on the role of structural variations on the organization of the binding sites conducive to silver cation binding characters of pyridine−amide macrocycles.

Design

The amide group in many hosts through N- -C═O- - - metal interactions directs the specificity of the host toward relatively soft alkaline earth cations, whereas ether−ester macrocyclic ionophores show high selectivity in complex formation with alkali metal ions. We found

[⊗] Abstract published in *Advance ACS Abstracts,* September 15, 1996.

(1) (a) An, H.; Bradshaw, J. S.; Izatt, R. M.; Yan, Z. *Chem. Rev.* **1994**, *94*, 939. (b) Gokel, G. W. *Chem. Soc. Rev.* **1992**, 39. (c) Izatt, R. M.; Bradshaw, J. S.; Pawlak, K.; Bruening, R. L.; Tarbet, B. J. *Chem. Rev.* **1992**, *92*, 1261. (d) An, H.; Bradshaw, J. S.; Izatt, R. M. *Chem. Rev.* **1992**, *92*, 543. (e) Izatt, R. M.; Pawlak, K.; Bradshaw, J. S.; Bruening, R. L. *Chem. Rev.* **1991**, *91*, 1721. (f) Mcdaniel, C. W.; Bradshaw, J. S.; Izatt, R. M. *Heterocycles* **1990**, *30*, 665. (g) Krakowiak, K. E.; Bradshaw, J. S.; Krakowiak, D. J. Z. *Chem. Rev.* **1989**, *89*, 929. (h) Cram, D. J. *Angew. Chem., Int. Ed. Engl.* **1988**, *27*, 1009. (i) Lehn, J. M. *Angew. Chem., Int. Ed. Engl.* **1988**, *27*, 89. (j) Cram, D. J. *Angew. Chem., Int. Ed. Engl.* **1986**, *25*, 1039. (k) Bradshaw, J. S.; Christensen, J. J.; Sen, D. *Chem. Rev.* **1985**, *85*, 272.

(2) (a) Hilgenfeld, R.; Saenger, W. *Topics in Current Chemistry*; Boschke, F. L., **1982**, *101*, 1−82. (b) Burger, H. M.; Seebach, D. *Angew Chem., Int. Ed. Engl.* **1994**, *33*, 442. (c) Wipf, P.; Venkataraman, S.; Miller, C. P.; Geib, S. J. *Angew. Chem., Int. Ed. Engl.* **1994**, *33*, 1516.

(3) Constable, E. C. In *Metals and Ligand Reactivity*; VCH Publishers: New York, 1996; p 66.

(4) (a) Cathala, B.; Picard, C.; Cazaux, C.; Tisnes, P.; Momtchev, M. *Tetrahedron* **1995**, *51*, 1245. (b) Pigot, T.; Duriez, M. C.; Cazaux, L.; Picard, C.; Tisnes, P. *J. Chem. Soc., Perkin Trans. 2* **1993**, 221. (c) Bell, T. W.; Choi, H.; Heil, G. *Tetrahedron Lett.* **1993**, *34*, 971. (d) Xh, X.; Stack, T. D. P.; Raymond, K. N. *Inorg. Chem.* **1992**, *31*, 4903. (e) Pierre, J. L.; Baret, P.; Gellon, G. *Angew. Chem., Int. Ed. Engl.* **1991**, *30*, 85.

(5) (a) Konig, B.; Moller, O.; Bubenitschek, P.; Jones, P. G. *J. Org. Chem.* **1995**, *60*, 4291. (b) Pernia, G. J.; Kilburn, J. D.; Rowley, M. *J. Chem. Soc., Chem. Commun.* **1995**, 305. (c) Waymark, C. P.; Kilburn, J. D.; Gillier, I. *Tetrahedron Lett.* **1995**, *36*(17), 3051. (d) Mitchell, M. C.; Cawley, A.; Kee, T. P. *Tetrahedran Lett.* **1995**, *36*, 287. (e) Hamura, Y.; Geib, S. J.; Hamilton, A. D. *Angew. Chem., Int. Ed. Engl.* **1994**, *33*, 446. (f) Hunter, C. A. *Chem. Soc. Rev.* **1994**, *23*, 101. (g) Brooksby, P. A.; Hunter, C. A.; Mcquillan, A. T.; Purvis, D. H.; Rowan, A. F.; Shannan, R. J.; Walsh, R. *Angew. Chem., Int. Ed. Engl.* **1994**, *33*, 2489.

(6) (a) Bryant, L. H.; Lachgar, A.; Jackels, S. C. *Inorg. Chem.* **1995**, *34*, 4230. Kim, W. D.; Hrncir, D. C.; Kiefer, G. E.; Sherry, A. D. *Inorg. Chem.* **1995**, *34*, 2225; (c) *J. Chem. Soc. Dalton Trans.* **1994**, 485.

(7) (a) Huszthy, P.; Oue, M.; Bradshaw, J. S.; Zhu, C. Y.; Wang, T.; Dalley, N. K.; Curtis, J. C.; Izatt, R. M. *J. Org. Chem.* **1992**, *57*, 5383. (b) Newcomb, M.; Gokel, G. W.; Cram, D. J. *J. Am. Chem. Soc.* **1974**, *96*, 6810. (c) Kaplan, L. J.; Weisman, G. R.; Cram, D. J. *J. Org. Chem.* **1979**, *44*, 2226.

(8) (a) Izatt, R. M.; Lamb, J. D.; Asay, R. E.; Maas, G. E.; Bradshaw, J. S.; Christensen, J. J. *J. Am. Chem. Soc.* **1977**, *99*, 6134. (b) Bradshaw, J. S.; Maas, G. E.; Lamb, J. D.; Izatt, R. M.; Christensen, J. J. *J. Am. Chem. Soc.* **1980**, *102*, 467. (c) Bradshaw, J. S.; Spencer, N. O.; Hemen, G. R.; Izatt, R. M.; Christensen, J. J. *J. Heterocycl. Chem.* **1983**, *20*(2), 353. (d) Izatt, R. M.; Lindh, G. C.; Clark, G. A.; Nakatsuzi, Y.; Bradshaw, J. S.; Lamb, J. D.; Christensen, J. J. *J. Membrane Sci.* **1987**, *31*, 1−13. (e) Lamb, J. D.; Izatt, R. M.; Swain, C. S.; Bradshaw, J. S.; Christensen, J. J *J. Am. Chem. Soc.* **1980**, *102*(2), 479. (f) Singh, H.; Kumar, S.; Jain, A. *J. Chem. Soc., Perkin Trans. 1* **1990**, 965.

(9) Wu, G.; Jiang, W.; Lamb, J. D.; Bradshaw, J. S.; Izatt, R. M. *J. Am. Chem. Soc.* **1991**, *113*, 6538.

S0022-3263(96)00859-6 CCC: $12.00

that pyridine−ether−ester macrocycles show significant selectivity for softer Ba^{2+} and Tl^{+} cations.[8] Hence, in order to induce binding selectivity for soft cations, we designed macrocycles I, II, and III possessing 2 × pyridine, 2 × amide, and 2 × ester moieties.

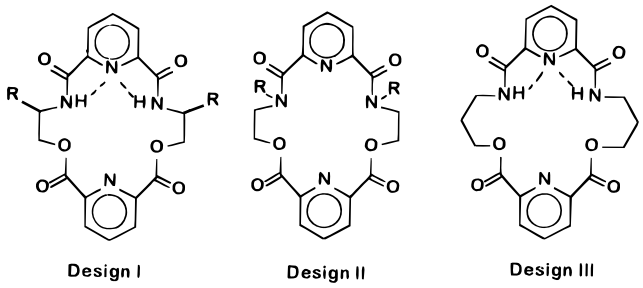

The CPK model of macrocycle design I shows a more or less planar structure, with two pyridine N and amide NH pointing toward the cavity with a strong possibility of amide NH hydrogen bonding with pyridine N. The substituent R does not affect the topology of the cavity, but the presence of alkyl substituent on each amide nitrogen in the design II, due to steric reasons, puts the alkyl groups out of the cavity and thus orients the amide units in such a way that the oxygens could be directed toward the cavity. Here, if two alkyl groups remain on the same side of the molecule, the two pyridine N and two amide oxygens make a well-defined spatial binding sphere, which is not observed when the alkyl groups are placed on the opposite side of the molecule. Thus, amide oxygens due to their relatively higher electron densities would preferably bind and induce enhanced selectivities toward softer cations. The bigger ring size in design III would increase the flexibility as well as lipophilicity of the molecules.

On the basis of these designs, we have synthesized six ionophores, two each related to the designs I−III, and have found that their structures in the solid state (X-ray) and in solution (^{1}H and ^{13}C NMR) by and large conform to the above observations. Although all the compounds have been found to exhibit a tendency to preferably bind softer cations, compounds derived from model II have remarkable selectivity toward silver cations.[10]

Synthesis

For the synthesis of macrocycle **9**, since the straightforward single-step condensation of pyridine−2,6-dicarbonyl dichloride (**1a**) with 2-aminoethanol, even when performed under phase transfer catalytic (PTC) conditions, gave a multitude of products, the following two-step approach, involving aminolysis of diethyl pyridine-2,6-dicarboxylate (**1b**) with amino alcohols to form diols (**3**−**8**) followed by intermolecular cyclodehydrochlorination of the latter and **1a**, was adopted (see Scheme 1).

Compound **1b** on heating with 2-aminoethanol (**2**, R^1, R^2 = H) gave diol **3** (90%), M^+ *m*/*z* 253. In its ^{1}H NMR spectrum, only one triplet and one quartet (which collapses to triplet on D_2O exchange) along with OH, NH, and Py−H signals appeared. In the ^{13}C NMR spectrum, in addition to the main expected signals for the symmetrical structure (**3**), low intensity signals (<10%), again conforming to structure **3** but indicating nonequivalence of pyC-3 and pyC-5, appeared. The latter could be attributed to a configurationally isomeric structure caused by amide units. Evidently, this isomer is present in such a low concentration that its presence is not detected in the ^{1}H NMR spectrum. The diol **3** on condensation with **1b** under PTC conditions gave **9** (35%), mp 324 °C, M^+, *m*/*z* 384. The number and multiplicity of signals in its ^{1}H and off-resonance ^{13}C NMR spectra pointed to its highly symmetrical structure. The ^{1}H NMR spectrum showed a sharp 2H signal at δ 3.1, for a water molecule, the presence of which was also evident from its elemental analysis.

Scheme 1

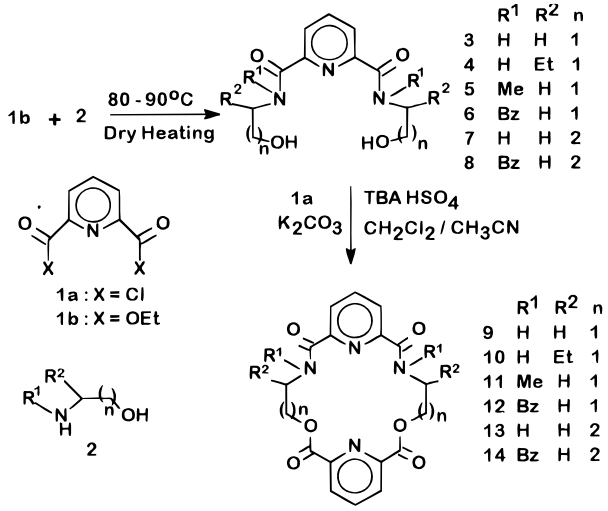

The reactions of **1b** with (−)-2-aminobutanol (**2**, *n* = 1, R^1 = H, R^2 = Et) and 3-aminopropanol gave diols **4** and **7**, respectively. The ^{1}H and ^{13}C NMR spectra of **4** depict its symmetrical structure and absence of any configurational isomer. The additional signals in the ^{13}C NMR spectrum of compound **7** that are not present in its ^{1}H NMR spectrum point to the presence of a small amount of a configurational isomer. The diols **4** and **7** on reactions with **1a** gave macrocycles **10** and **13**, respectively. The ^{1}H and ^{13}C NMR spectra of **10** and **13** corroborrate their symmetrical organized structures. The splitting pattern of OCH_2 in the ^{1}H NMR of **10** is influenced by the adjacent assymetric methine H. The ^{1}H NMR spactra also depict the presence of a strongly bonded water molecule in each case. Therefore, the macrocycles **9**, **10**, and **13** have electron-deficient cavities and a substituent on two carbon spacer unit in **10** as well as its extension to three carbon spacer in **13** has not apparently affected the structural pattern adopted by the parent macrocycle **9**.

N-Methyl-2-aminoethanol and **1b** react to form the diol **5**, which in its ^{1}H NMR spectrum shows two singlets at δ 3.04 and 3.17 (3H each) due to NCH_3 and two triplets at δ 3.56 (2H) and δ 3.69 (2H) due to NCH_2 and a triplet at δ 3.87 (4H) along with 3pyH multiplet and OH (2H) signals. Its ^{13}C NMR spectrum also shows two equal intensity signals due to NCH_3, NCH_2, and OCH_2 carbons along with three pyCH and two pyC-2 and two CON carbons. These data firmly point to the existence of **5** as two configurational isomers in equal amounts. The condensation of **5** with **1a** gave the macrocycle **11** (45%), M^+ *m*/*z* 412. Its ^{1}H NMR spectrum shows only one

(10) Preliminary communications: (a) Kumar, S.; Singh, R.; Singh, H. *Bioorg. Med. Chem. Letts.* **1993**, *3*, 363. (b) Kumar, S.; Hundal, M. S.; Kaur, N.; Singh, R.; Hundal, G.; Ripoll, M. M.; Aparicio, J. S. *Tetrahedron Lett.* **1995**, *36*, 9543.

signal due to NCH_3 and broad multiplets for NCH_2, OCH_2, and pyH. Unlike macrocycles **9**, **10**, and **13**, its ^1H NMR and elemental analysis did not show the presence of a water molecule. The proton-decoupled off-resonance ^{13}C NMR spectrum of **11** shows one quartet and two triplets in the aliphatic region. These data point to a highly rigid but a symmetrical structure for compound **11**, at least in solution phase with both of its two NCH_3 groups positioned on the same side of the plane of the molecule. The absence of a water molecule, which could be ascribed to lack of the possibility of H-bonding of tertiary amide, is evidently responsible for the electron-rich nature of the system.

The diol **6** formed from *N*-benzyl-2-aminoethanol and **1b** shows configurational isomerism from its NMR data. The reaction of **1a** and **6** gave macrocycle **12**, which again, like its analog **11**, from its ^1H and ^{13}C NMR data shows an organized symmetrical electron-rich configuration.

A TLC homogeneous sample of diol **8** formed from *N*-benzyl-3-aminopropanol and **1b**, shows in its NMR data a more pronounced configurational isomerism arising because of the size of the benzyl substituent. The macrocycle **14** formed from **8** and **1a** shows in its ^1H NMR spectrum multiple signals all due to CH_2 and aromatic H. Its ^{13}C NMR shows three signals, each due to $-CH_2-$ (δ 24.57, 25.14, 26.46), $-NCH_2-$ (δ 42.53, 42.75, 43.88), OCH_2 (δ 46.07, 48.11, 51.94), and NCH_2-Ph (δ 60.77, 62.75, 66.68), along with more than two signals due to each Py and aromatic carbons and two signals each due to amide C=O (δ 163.97, 164.41) and ester C=O (δ 168.22, 169.51). Probably due to the presence of more flexible spacers and the bulkier N-substituents, various structural units of macrocycle **14** adopt different configurational and conformational dispositions in solution which are responsible for the appearance of multitude of signals for even chemically equivalent species.

For the synthesis of macrocycle **16** (n = 0, 1, 2), with the objective of identifying the role of pyridine N of the ester unit, on the ionophore character of macrocycles **9**−**14**, the cyclization of the diols **3**, **5**, and **7** with 1,2-dibromoethane, 1,3-dibromopropane, and 1,4-dibromobutane were attempted under phase transfer catalytic conditions (K_2CO_3, TEBA, CH_3CN, stirring at 90−95 °C). With the exception of **7**, which on its reaction with 1,3-dibromopropane formed a new product, mp 250 °C, mol wt 307, all other reactions were unsuccessful. The spectral data showed the incorporation of $-OC(O)O-$ rather than a $-O(CH_2)_3O-$ unit in the precursor diol. The carbonate unit evidently could be incorporated by the base used in the reaction. But a blank reaction run on **7** in the absence of 1,3-dibromopropane did not provide **16** depicting a decisive role for the dihalide in the mode of the reaction. The formation of **15** could be visualized to proceed through the PTC-catalyzed conversion of 1,3-dibromopropane with potassium carbonate to propylene carbonate followed by its reaction with diol **7**. This mechanism is further supported by the formation of **15** along with unidentified product by the reaction of **7** with diethyl carbonate and the poor reactivity of **7** toward ethylene carbonate. But, the diol **5** under phase-transfer catalytic conditions (CH_2Cl_2−NaOH−$TBAHSO_4$) reacted with dichloromethane to give macrocycle **17**. The scope of such reactions of diols for developing the synthetic methodology for macrocyclic carbonates is being studied.

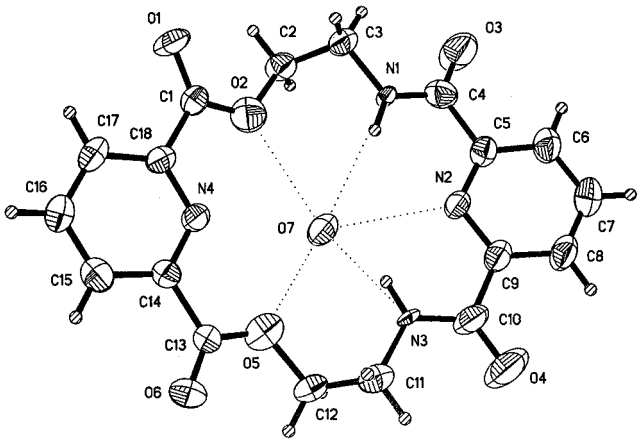

Figure 1. ORTEP view of macrocycle **9**. Thermal ellipsoids are drawn with 50% probability, and hydrogen atoms are drawn with arbitrary small isotopic thermal parameters for sake of clarity. Hydrogens attached to O7 were not located in the difference Fourier. All possible short distances between O7 and other donors are indicated by dotted lines.

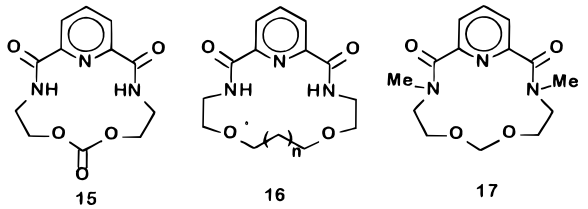

Crystal Structure Discussion

The NMR spectral features group these macrocycles (**9**−**14**) in three distinct categories: (i) planar, water-encapsulating electron-deficient **9, 10**, and **13** and three-dimensional electron-rich macrocycles (ii) **11** and **12** and (iii) **14**, bearing two and three carbon spacers, respectively. Hence, solid state structures of their representatives **9**, **11**, and **14** were determined by X-ray diffraction studies.

The X-ray structure of **9** reveals a water molecule H-bonded to the macrocycle. Since hydrogen atoms of water could not be located, all possible intramolecular contacts are shown in Figure 1. The only short intermolecular contact is between O7- -$O1^i$ ($i = x, -y + 1/2, z - 1/2$). The amide groups N1−C4−O3 and N3−C10−O4 are twisted by 14.3(2)° and 2.8(2)° with respect to the pyridine ring. The two ester O, two pyN, and two amide nitrogens are pointing inward and amide oxygens are pointing outward from the cavity. The presence of a water molecule in the macrocycle causes the amide groups to adopt a conformation in which they are only slightly twisted with respect to the pyridine rings and permits the macrocycle to acquire a flattened conformation. The substitution of a methyl group at each of the amide groups in the 18-membered ring in **11** causes significant changes in the conformation of the macrocycle (Figure 2). The amide groups N1−C5−O3 and N3−C11−O4 are twisted around N1−C5−O3 and N3−C11−O4 by 61.9(2)° and 48.8(2)°, respectively. The two carboxyl groups make dihedral angles of 21.0(2)° and 28.6(2)° with the pyridine ring. In this structure two amide oxygens lie on the same side of the mean plane of the pyridine ring. Since the amide groups are highly twisted with respect to the pyridine there is no delocalization of the electron density between amide groups and pyridine ring. So, relatively free adjustment of torsion angles is possible

Table 1. Metal Ion Extraction Profile (Percent Extraction) of Macrocycles 9−14[a]

compd. no.	Li^+	Na^+	K^+	Mg^{2+}	Ca^{2+}	Sr^{2+}	Ba^{2+}	Tl^+	Pb^{2+}	Ag^+	Ag^+/Pb^{2+}	Ag^+/Tl^+
9	3.08	3.37	3.34	2.43	3.72	3.84	3.36	3.43	18.65	7.07	0.38	2.06
10	0.26	0.34	0.35	0.08	0.09	0.09	−	0.38	0.78	1.23	1.58	3.24
11	−	−	−	−	−	1.30	−	0.37	0.89	56.20	63.15	151.9
12	0.20	0.20	0.10	0.10	0.10	0.10	−	0.60	0.5	66.40*	132.8	110.6
13	0.50	0.50	0.50	0.30	0.30	0.40	0.30	0.60	3.0	4.40	1.50	7.20
14	0.10	0.10	0.10	0.10	0.20	0.30	−	0.20	3.50	0.67	1.92	33.50

[a] − indicates that the ion was not extracted. *Separation of solid−macrocycle complex.

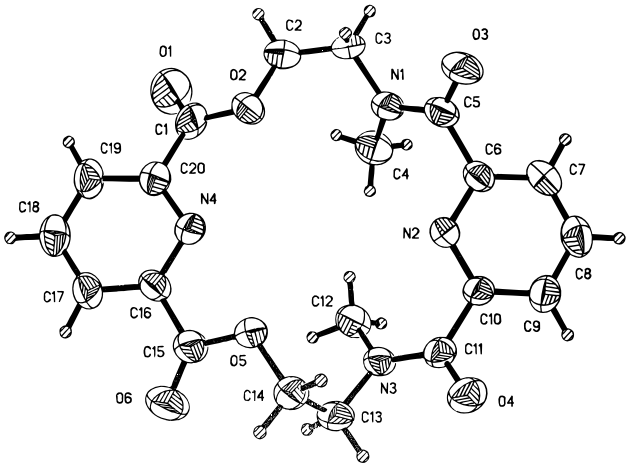

Figure 2. ORTEP view of macrocycle **11**. Thermal ellipsoids are drawn with 50% probability, and hydrogen atoms are drawn with arbitrary small isotopic thermal parameters for sake of clarity.

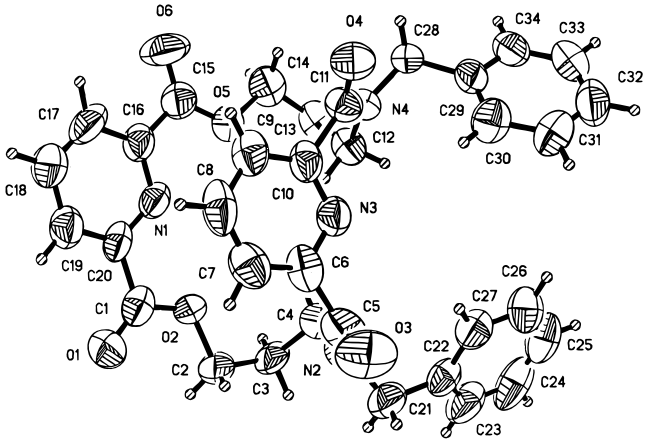

Figure 3. ORTEP view of macrocycle **14**. Thermal ellipsoids are drawn with 50% probability, and hydrogen atoms are drawn with arbitrary small isotopic thermal parameters for sake of clarity.

during complexation. In the free ligand the two amide oxygens and pyridine nitrogen form a T-shaped site. On slight rotation about the C10−C11 and C5−C6 bonds the macrocycle can offer two pyridine nitrogens and two amide oxygens for complexation with a metal ion—a prerequisite of 2−4 coordination sites for selective Ag^+ binding. The twist of the amide group with respect to the pyridine ring system constitutes an interesting feature of the macrocycle **11** as both amide oxygens lie on the same side of the pyridine ring.

The X-ray structure of **14** shows a complete change in the topology of the molecule. The amide groups are twisted with respect to the pyridine mean plane by 43.1(5)° and 48.8(5)°, whereas the carboxyl groups are making dihedral angles of 6.3(4)° and 9.6(6)°. The benzyl group substituent at the amide nitrogen takes the amide oxygens O3 and O4 in a direction away from the macrocycle cavity such that a rotation of 180° is needed to bring the amide oxygen into the cavity (Figure 3). Due to this lop-sided change in the configuration, **14** lacks the cavity and binding character. Therefore, the combined effect of both the longer spacer (propylene unit) and the bulky benzyl groups adversely affect the binding character.

Thus, although there is always a possibility for the macrocycles to have different conformational structures in the solid state and in the solution phase, here the solid state structure analysis conforms to the conformational features as could be derived from the NMR studies in solution phase.

Binding Characters

Extraction and Transport Studies. As the process of ligand-facilitated transport of cations across a nonpolar membrane has the relevance to development of separation techniques for cations, the extraction[11] (complexation) and transport[12] (complexation/decomplexation) profiles of macrocycles **9**−**14** toward Ag^+, Pb^{2+}, Tl^+, alkali metal cations (Li^+, Na^+, K^+) and alkaline earth cations (Mg^{2+}, Ca^{2+}, Sr^{2+}, Ba^{2+}) by using chloroform as apolar membrane have been determined.

The compound **9**, which has a more or less planar structure and a cavity that remains preoccupied with one water molecule, shows 18.65 and 7.07% extraction of Pb^{2+} and Ag^+ picrates, respectively, whereas other metal picrates are also extracted (2.5−3.5%), leading to poor selectivity toward Pb^{2+}. The presence of an ethyl substituent on the carbon spacer in **10** or the increase in spacer length in **13** does not affect their complexation toward water but adversely affects the extraction of all the cations (Table 1). The presence of a methyl substituent on the amide N in macrocycle **11** leads to a highly organized structure (X-ray and ^1H NMR), and it extracts nearly 54% of Ag^+ picrate from the aqueous phase, whereas other cations are extracted by less than 1%. A further increase in the size of the substituent on the amide N in **12** further increases the extraction of Ag^+ (66%). Consequently, **12** extracts Ag^+ nearly 132 times more than Pb^{2+} and much more than other cations. Here, the steric restriction of methyl/benzyl groups in the formation of 2:1 (L:M) complexes, required for binding with other cations, also helps in lessening the extraction of cations other than Ag^+. In macrocycle **14**, the combined effect of increase in substituent size and spacer length leads to lopsided reversion in configuration and

(11) (a) Moore, S. S.; Tarnowski, T. L.; Newcomb, M.; Cram, D. J. *J. Am. Chem. Soc.* **1977**, *99*, 6398. (b) Koenig, K. E.; Lehn, G. M.; Stuckler, P.; Kaneda, T.; Cram, D. J. *Ibid.* **1979**, *101*, 3553.

(12) (a) Maruyama, K.; Tsukube, H.; Akai, T. *J. Am. Chem. Soc.* **1980**, *102*, 3246. (b) Maruyama, K.; Tsukube, H.; Akai, T. *J. Am. Chem. Soc., Dalton Trans.* **1981**, 1486.

Table 2. Metal Ion Transport Rates Profiles ($\times 10^7$ Mol/24 h) of Macrocycles 9−14[a]

compd no.	Li^+	Na^+	K^+	Mg^{2+}	Ca^{2+}	Sr^{2+}	Ba^{2+}	Tl^+	Pb^{2+}	Ag^+	Ag^+/Tl^+
9	3.7	4.4	3.1	3.1	4.0	0.0	3.1	5.7	−	7.0	1.2
10	26.2	18.2	43.0	19.4	27.8	0.0	11.6	88.8	−	192.5	2.2
11	1.2	2.7	2.2	3.0	2.0	0.0	1.5	11.5	−	543.0	47.2
12	5.9	6.4	7.2	5.9	8.0	7.3	10.8	24.9	−	372.8*	15.0
13	2.4	2.0	2.2	0.3	0.2	0.1	0.4	4.4	−	234.4	53.0
14	1.3	1.2	7.2	0.9	11.8	10.8	4.8	16.1	−	330.5	20.5

[a] − indicates that the rate profile could not be determined due to significant leakage. *Separation of solid silver−macrocycle complex.

Table 3. ^{13}C NMR Coordination Shifts[a] ($\Delta\delta$) for Macrocycles 9 and 11

	macrocycle **9**				macrocycle **11**			
signal	Ag^+	Pb^{2+}	Tl^+	Sr^{2+}	Ag^+	Pb^{2+}	Tl^+	Sr^{2+}
NCH_3	−	−	−	−	−*	−0.11	−0.64	−0.01
NCH_2	+0.07	+0.00	−0.03	0.00	−1.03	−0.07	−0.54	−0.01
OCH_2	−0.09	+0.11	+0.03	+0.22	−0.80	−0.06	−0.54	−0.02
pyc-3	+0.19	+0.03	−0.01	+0.07	−1.09	−0.01	−0.43	+0.08
pyc-3	+0.23	+0.08	+0.04	+0.15	+1.49	+0.08	−0.12	+0.11
pyc-4	+0.17	+0.01	+0.01	+0.01	+2.01	−0.00	−0.17	+0.14
pyc-4	+0.30	+0.12	+0.05	+0.22	+1.81	+0.12	−*	−*
pyc-2	+0.01	−0.01	−0.04	−0.01	−0.58	−0.05	−0.47	−0.03
pyc-2	+0.28	−0.02	−0.04	−0.05	+3.87	+0.05	−*	+0.01
CO	+0.28	+0.11	+0.02	+0.20	−*	+0.04	−0.28	+0.04
CO	−0.19	−*	−0.02	−0.05	+0.79	−*	−0.14	−*

[a] Conditions: macrocycle (0.049 mmol); metal picrate (0.049 mmol) in DMF−$CDCl_3$ (1:1, v:v; 1 mL). Positive is downfield shift. *Could not be detected. For other metal picrates changes in chemical shifts are <0.05.

places the amide oxygen and pyridine N out of the cavity in different directions and thus shows poor extraction of cations.

Thus, compounds **9**, **10**, and **13**, which have electron-deficient cavities, in general show poor extraction of all the cations, and the macrocycles **11** and **12**, with well-defined electron-rich cavities due to steric restrictions in formation of 2:1 (L:M) complexes, show selective extraction of Ag^+ picrate.

The transport rates for Pb^{2+} picrate could not be determined because of its significant leakage. All these macrocycles show some selectivity toward the Ag^+ cation. The macrocycles **9** and **10**, which show poor selectivity in extraction, also show poor selectivity in transport character. The higher transport rates induced by **10** may be attributed to its higher lipophilicity than **9**. The macrocycle **13**, which is more flexible than **9** and **10**, shows significant selectivity toward Ag^+ over Tl^+ and other cations (Table 2). The macrocycle **11** transports Ag^+ picrate 47 times more than Tl^+, whereas other cations are practically not transported. Also, whereas transport rates for all the metal picrates increase linearly with respect to time, Ag^+ shows a steep fall in its transport rate after 3 h. On considering the transport rates at 3 h, **11** shows transport selectivity of the order of >100 toward Ag^+ as compared to Tl^+ and >2000 times than other metal picrates. In the case of compound **12**, during transport experiments, solid separation due to Ag^+−**12** complex formation takes place. The analysis of both aqueous and organic layers for the free silver picrate shows that only 30% of **12** remains active in case of Ag^+, and also, the transport rate is linear on time scale upto 4.5 h and then it falls significantly. Therefore, compounds **11** and **12** effectively have much higher transport selectivities than shown in Table 2. Macrocycle **14** also shows a high order of transport rate and selectivity toward Ag^+. Such a character could not be justified from its solid state structure. Probably, in solution phase, **14** exists in a number of conformations (also evident from its ^1H NMR), and one of these conformations may be responsible for silver transport. Since the ionophore-induced cation transport depends on both complexation and subsequent decomplexation of the cation, some anomalies in comparison to extraction results are evident.

Complexation Studies through ^{13}C NMR Spectroscopy. The comparison of ^{13}C NMR spectra of macrocycles with those of their 1:1 stoichiometric mixtures with metal picrates could give significant information about the complexation character of individual ligating sites and thus the macrocycles. For these studies, because in ^{13}C NMR, the signals due to pyridine−amide and pyridine−ester units, appear quite close to each other, their coordination shifts are interpreted as those of units and not of individual carbons.

The significant changes observed in the chemical shifts of macrocycles **9** and **11** on addition of Ag^+ and quite small changes on addition of other metal picrates show the higher order of binding of Ag^+ with both **9** and **11** in comparison with other cations. These findings are in consonance with extraction and transport results, with the exception of higher complexation of Ag^+ over Pb^{2+} in ^{13}C NMR studies that could be attributed to the difference in medium (DMF−$CDCl_3$ in ^{13}C NMR studies and $CHCl_3$−water biphase in extraction) in both cases. Further, the much higher magnitude of change in chemical shift in case of **11**−Ag^+ complexation ($\Delta\delta$ 0.58−3.87) over **9**−Ag^+ complexation ($\Delta\delta$ 0.07−0.30) depicts stronger binding in case of former (Table 3). These results highlight the participation of both the pyridine units in complexation with Ag^+. But, the participation of amide and esters could not be rationalized on the basis of ^{13}C NMR studies.

In conclusion, macrocycles **9**, **10**, and **13**, which have more or less planar structures, $N_{Py}\cdots HN_{amide}$ intramolecular hydrogen bonding, and encapsulate one water molecule in the cavity, during complexation have to undergo significant conformational changes and show poor complexation. But macrocycles **11** and **12**, where amide C═O are positioned toward the cavity, may undergo fewer conformational changes during complex-

ation and show high extraction of Ag^+. In analogy with recently reported results on a silver-selective triamide marine compound,[2c] which undergoes rotation during complexation to make amide oxygen available for silver binding, here in macrocycles **11** and **12**, the steric disposition of the N-substituent has induced conformational changes similar to the silver−triamide complex. Since the ionophore-induced cation transport depends on both complexation and subsequent decomplexation of the cation, some anomalies in comparison to extraction results are evident.

Experimental Section

General experimental details are given in ref 13.

Synthesis of Diols 3−8: Condensation of Diethyl Pyridine−2,6-dicarboxylate (1b) with 2-Aminoethanol, 2-Aminobutanol, *N*-Methyl-2-aminoethanol, *N*-Benzyl-2-aminoethanol, 3-Aminopropanol-1, and *N*-Benzyl-3-aminopropanol-1, Respectively. General Procedure. Diethyl pyridine-2,6-dicarboxylate (**1b**) (1 g, 4.4 mmol) was mixed with 2 equivalents of 2-aminoethanol (0.54 g, 8.8 mmol) and heated at 80−90 °C for 4−5 h. The ethanol formed during the reaction was stripped off under vacuum. A white solid product obtained was washed with chloroform (10 mL) and was recrystallized from ethanol to get pure **3** (90%). Similarly, other diols **4**−**8** were obtained in >90% yields.

***N,N′*-Bis(2-hydroxyethyl)-2,6-carboxamide (3):** 92% yield; mp 162 °C(EtOH); IR ν_{max} (KBr) cm^{-1} 3400, 1660; ^1H NMR [$CDCl_3$ + $(CD_3)_2SO$] δ (ppm) 3.00 (4 H, q, J = 5 Hz, collapses to triplet on D_2O exchange), 3.14−3.54 (2 H, br, exchanges with D_2O), 3.76 (4 H, t, J = 5 Hz), 7.99−8.07 (2 H, m), 8.26−8.34 (1 H, m), 9.22 (2 H, t, J = 6 Hz, exchanges with D_2O); ^{13}C NMR [$CDCl_3$ + $(CD_3)_2SO$] δ (ppm) 40.65 (t), 58.92 (t), 122.68 (d), 137.18 (d), 147.46 (s), 162.29 (s) [other small signals (10% intensity of the main signals) are at 40.34 (t), 56.55 (t), 120.97 (d), 124.60 (d), 136.12 (d), 163.21 (s)]; MS m/z 253 (M^+, 3). Anal. Calcd for $C_{11}H_{15}N_3O_5$: C, 51.78; H, 5.36; N, 16.02. Found: C, 52.1; H, 5.3; N, 16.3.

***N,N′*-Bis(1-ethyl-2-hydroxyethyl)-2,6-pyridinecarboxamide (4):** 93% yield; mp 160 °C (ethanol); $[\alpha]^{20}_D$ +57.9° (*c* 1.0, ethanol); IR ν_{max} (KBr) cm^{-1} 3300, 1675, 1640; ^1H NMR [$CDCl_3$ + $(CD_3)_2SO$] δ (ppm) 0.98 (6 H, t, J = 7.5 Hz), 1.72 (4 H, m), 3.61−3.75 (4 H, m), 3.92−4.05 (2 H, m), 4.30 (2 H, br, exchanges with D_2O), 7.88−8.28 (3 H, m), 8.55 (2 H, d, J = 8.5 Hz, exchanges with D_2O); ^{13}C NMR [$CDCl_3$ + $(CD_3)_2SO$] δ (ppm) 9.47 (q), 22.72 (t), 51.94 (d), 61.78 (t), 123.14 (d), 137.38 (d), 147.88 (s), 162.14 (s); MS m/z 309 (M^+ missing), 280 ($M^+ - CH_2CH_3$, 4). Anal. Calcd for $C_{15}H_{23}N_3O_4$: C, 58.25; H, 7.44; N, 13.59. Found: C, 58.2; H, 7.6; N, 13.7.

***N,N′*-Bis(2-hydroxyethyl)-*N,N′*-dimethyl-2,6-pyridinecarboxamide (5):** 95% yield; liquid; IR ν_{max} (KBr) cm^{-1} 3380, 1665; ^1H NMR [$CDCl_3$] δ (ppm) 3.04 (3 H, s), 3.17 (3 H, s), 3.56 (2 H, t, J = 5 Hz), 3.69 (2 H, t, J = 5 Hz), 3.87 (4 H, t, J = 5 Hz), 4.65−5.16 (2 H, b, exchanges with D_2O), 7.70−8.14 (3 H, m); ^{13}C NMR ($CDCl_3$) δ (ppm) 33.27 (q), 39.18 (q), 51.69 (t), 51.90 (t), 58.56 (t), 59.73 (t), 124.86 (d), 126.30 (d), 139.75 (d), 150.95 (s), 151.69 (s), 167.50 (s), 167.81 (s) [other small signals are at 52.22 (t), 52.32 (t), 58.81 (t), 128.65 (d), 138.76 (s)]; MS m/z 281 (M^+, 3), 250.

***N,N′*-Bis(2-hydroxyethyl)-*N,N′*-dibenzyl-2,6-pyridinecarboxamide (6):** 95% yield; liquid; IR ν_{max} (KBr) cm^{-1} 3380, 1628; ^1H NMR ($CDCl_3$) δ (ppm) 2.76 (2 H, t, J = 5 Hz), 3.48−3.67 (4 H, m), 3.80 (2 H, s), 3.84−3.88 (2 H, m), 4.26 (2 H, s, exchanges with D_2O), 4.67, 4.83 (2 H, s), 7.25−7.35 (10 H, m), 7.71−7.97 (3 H, m); ^{13}C NMR ($CDCl_3$) δ (ppm) 48.04 (t), 48.45 (t), 48.59 (t), 49.09 (t), 53.17 (t), 53.91 (t), 58.33 (t), 58.70 (t), 59.67 (t), 60.01 (t), 124.03 (d) 124.62 (d), 126.25 (d), 126.71 (d), 127.32 (d), 127.45 (d), 127.81 (d), 128.40 (d), 136.02 (s), 136.2 (s), 138.41 (d), 139.53 (d), 150.99 (s), 151.30 (s), 152.32 (s), 152.49 (s), 167.47 (s), 168.23 (s), 168.48 (s), 168.86 (s); MS m/z 433 (missing), 402 ($M^+ - CH_2OH$, 1).

***N,N′*-Bis(3-hydroxypropyl)-2,6-pyridinecarboxamide (7):** 94% yield; mp 110 °C (EtOH); IR ν_{max} (KBr) cm^{-1} 3300, 1660; ^1H NMR [$CDCl_3$ + $(CD_3)_2SO$] δ (ppm) 1.84 (4 H, quint, J = 6 Hz), 3.56 (4 H, q, J = 6 Hz, changes to triplet on D_2O exchange), 3.65 (4 H, t, J = 6 Hz), 4.57 (2 H, br, exchanges with D_2O), 8.01−8.27 (3 H, m), 9.21−9.27 (2 H, t, J = 6 Hz, exchanges with D_2O); ^{13}C NMR [$CDCl_3$ + $(CD_3)_2SO$] δ (ppm) 30.99 (t), 35.16 (t), 57.68 (t), 122.67 (d), 137.33 (d), 147.47 (s), 162.26 (s) [other small signals (10% intensity of the main signals) are at 29.95 (t), 34.90 (t), 120.79 (d), 136.05 (d)]; MS m/z 281 (M^+, 3). Anal. Calcd $C_{13}H_{19}N_3O_4$: C, 55.51; H, 6.76; N, 13.94. Found: C, 55.3; H, 7.0; N, 13.7.

***N,N′*-Bis(3-hydroxypropyl)-*N,N′*-dibenzyl-2,6-pyridinecarboxamide (8):** 93% yield; thick liquid; IR ν_{max} (KBr) cm^{-1} 3410, 1622; ^1H NMR ($CDCl_3$) δ (ppm) 1.68−2.04 (4 H, m), 2.97 (2 H, t, J = 6 Hz), 3.48−3.71 (6 H, m), 3.93 (2 H, s, exchanges with D_2O), 4.74 (2 H, s), 4.80 (2 H, s), 7.13−7.42 (10 H, m), 7.73−8.15 (3 H, m); ^{13}C NMR ($CDCl_3$) δ (ppm) 29.53 (t), 30.66 (t), 42.22 (t), 45.21 (t), 46.55 (t), 48.17 (t), 52.20 (t), 58.37 (t), 58.83 (t), 61.17 (t), 61.70 (t), 62.09 (t), 125.65 (d), 125.76 (d), 127.55 (d), 127.92 (d), 128.13 (d), 128.46 (d), 128.87 (d), 136.3 (s), 136.41 (s), 136.72 (s), 138.05 (d), 138.16 (d), 145.9 (d), 146.5 (d), 152.30 (s), 153.7 (s), 154.36 (s), 164.46 (s), 167.86 (s), 168.61 (s), 168.97 (s); MS m/z 461 (M^+, 1), 417, 297.

Synthesis of Macrocycles 9−14. General Procedure. To a stirred mixture of anhydrous K_2CO_3 and tetrabutylammonium hydrogen sulfate (10 mg) in dry acetonitrile or dichloromethane (600−700 mL) were added a solution of diol **3** (1.0 g, 3.9 mmol) in dry acetonitrile or dichloromethane (60−70 mL) and a solution of pyridine-2,6-dicarbonyl dichloride (1.0 g, 4.1 mmol) in dry acetonitrile or dichloromethane simultaneously dropwise, and stirring was continued at room temperature. After completion of the reaction (TLC, 7 h), the suspension was filtered off and the residue was washed with ethyl acetate. The combined filtrate and washings were distilled off, and the crude reaction product was chromatographed over silica gel column using chloroform−ethyl acetate mixtures as eluents to isolate pure macrocycle **9**. Similarly, compounds **4**−**8** with pyridine-2,6-dicarbonyl dichloride under the same conditions gave macrocycles **10**−**14,** respectively.

In an alternate attempt, the direct synthesis of macrocycle **9** was accomplished by cyclodehydrohalogenation of **1a** (1.0 g, 4.1 mmol) and 2-aminoethanol (0.25 g, 4.1 mmol) in dry CH_2Cl_2 using K_2CO_3 as base and $TBAHSO_4$ as catalyst. However, the product could be isolated only in 12% yield.

5,14-Dioxa-2,17-diaza[6,6](2,6)pyridinophane-1,6,13,18-tetrone (9): 35% yield; mp 324 °C (CH_2Cl_2−ether); IR ν_{max} (KBr) cm^{-1} 3420, 1725, 1670; for vacuum-dried sample at 120 °C; ^1H NMR ($CDCl_3$) δ (ppm) 3.10 (2 H, s, exchanges with D_2O), 3.97 (4 H, q, J = 5 Hz, collapses to triplet on D_2O exchange), 4.64 (4 H, t, J = 5 Hz), 8.01−8.13 (2 H, m), 8.32−8.44 (4 H, m), 9.10 (2 H, t, J = 6 Hz, exchanges with D_2O); ^{13}C NMR ($CDCl_3$) δ (ppm) 42.26 (t), 65.53 (t), 124.9 (d), 138.78 (d), 138.9 (d), 147.97 (s), 148.57 (s), 163.52 (s), 164.23 (s). MS m/z 384 (M^+, 100). Anal. Calcd for $C_{18}H_{16}N_4O_6 \cdot H_2O$: C, 53.73; H, 4.48; N, 13.93. Found: C, 53.3; H, 4.1; N, 13.6. Anal. Calcd for $C_{18}H_{16}N_4O_6$: C, 56.25; H, 4.16; N, 14.58. Found: C, 56.5; H, 4.0; N, 14.2.

(−)-3,16-Diethyl-5,14-dioxa-2,17-diaza[6,6](2,6)pyridinophane-1,6,13,18-tetrone (10): 33% yield; mp 204 °C (CH_2Cl_2−ether); IR ν_{max} (KBr) cm^{-1} 3400, 1730, 1665; for vacuum-dried sample at 120 °C, ^1H NMR ($CDCl_3$) δ (ppm) 1.00 (6 H, t, J = 7.5 Hz), 1.60−1.86 (4 H, m), 2.93 (2 H, b, exchanges with D_2O), 4.23 (2 H, dd, J = 2 Hz, $\Delta\delta$ 11.4 Hz), 4.48−4.60 (2 H, m), 5.22 (2 H, dd, J = 2 Hz, $\Delta\delta$ 11.4 Hz), 8.02−8.44 (6 H, m), 8.62−8.67 (2 H, d, J = 10 Hz, exchanges with D_2O); ^{13}C NMR ($CDCl_3$) δ (ppm) 10.74 (q), 24.57 (t), 50.15 (d), 66.59 (t), 125.44 (d), 128.64 (d), 138.34 (d), 138.77 (d), 147.79 (s), 148.91 (s), 163.22 (s), 164.62 (s); MS m/z 440 (M^+, 63). Anal. Calcd for $C_{22}H_{24}N_4O_6 \cdot H_2O$: C, 47.16; H, 5.68; N, 12.23. Found: C, 47.3; H, 5.6; N, 12.0. Anal. Calcd for $C_{22}H_{24}N_4O_6$: C, 60.00; H, 5.45; N, 12.72. Found: C, 60.3; H, 5.5; N, 12.4.

5,14-Dioxa-2,17-*N,N*-dimethyldiaza[6,6]pyridinophane-1,6,13,18-tetrone (11): 45% yield; mp 205 °C (CH_2Cl_2−ether);

(13) Singh, H.; Singh, P.; Chimni, S. S.; Kumar, S. *J. Chem. Soc., Perkin Trans. 1* **1995**, 2363.

IR ν_{max} (KBr) cm^{-1} 1728, 1628; ^1H NMR ($CDCl_3$) δ (ppm) 3.46 (6 H, s), 3.90−4.10 (4 H, m), 4.60−4.95 (4 H, m), 7.86−8.38 (6 H, m); ^{13}C NMR ($CDCl_3$) δ (ppm) 41.93 (q), 49.18 (t), 64.15 (t), 124.99 (d), 128.17 (d) 138.03 (d), 138.25 (d), 148.54 (s), 151.70 (s), 165.21 (s), 167.91 (s); MS *m*/*z* 412 (M^+, 99). Anal. Calcd for $C_{20}H_{20}N_4O_6$: C, 58.25; H, 4.85; N, 13.59. Found: C, 58.3; H, 4.9; N, 13.6.

5,14-Dioxa-2,17-*N*,*N*-dibenzyldiaza[6,6]pyridinophane-1,6,13,18-tetrone (12): 32% yield; mp 212 °C (CH_2Cl_2−ether); IR ν_{max} (KBr) cm^{-1} 1720, 1635; ^1H NMR ($CDCl_3$) δ (ppm) 3.19 (4 H, m), 4.48−4.62 (4 H, m), 5.52 (2 H, s), 5.66 (2H, s), 6.91−7.26 (10 H, m), 7.79−8.41 (6 H, m); ^{13}C NMR ($CDCl_3$) δ (ppm) 45.34 (t), 55.69 (t), 64.21 (t), 124.99 (d), 127.47 (d), 128.21 (d), 128.62 (d), 137.32 (s), 138.07 (d), 138.56 (d), 148.70 (s), 151.80 (s), 161.26 (s), 168.85 (s); MS *m*/*z* 564 (M^+, 18). Anal. Calcd for $C_{32}H_{28}O_6N_4$: C, 68.09; H, 4.96; N, 9.93. Found: C, 68.0; H, 4.8; N, 9.9.

6,15-Dioxa-2,17-diaza[7,7]pyridinophane-1,7,14,20-tetrone (13): 20% yield; mp 245 °C (CH_2Cl_2−ether); IR ν_{max} (KBr) cm^{-1} 3400, 1725, 1670; ^1H NMR ($CDCl_3$) δ (ppm) 1.85 (4 H, q, J = 6 Hz), 2.50 (2 H, b, exchanges with D_2O), 3.65 (4 H, q, J = 6 Hz, collapses to triplet on D_2O exchange), 3.85 (4 H, t, J = 6 Hz), 7.93−8.01 (2 H, m), 8.22−8.26 (4 H, m), 8.83 (2 H, t, J = 6 Hz, exchanges with D_2O); ^{13}C NMR ($CDCl_3$) δ (ppm) 30.86 (t), 54.21 (t), 57.23 (t), 120.76 (d), 122.96 (d), 137.13 (d), 146.93 (s), 161.29 (s), 162.69 (s); MS *m*/*z* 412 (M^+, 88). Anal. Calcd for $C_{20}H_{20}N_4O_6 \cdot H_2O$: C, 55.8; H, 5.12; N, 13.02. Found: C, 55.5; H, 5.2; N, 13.3.

6,15-Dioxa-2,17-*N*,*N*-dibenzyldiaza[7,7]pyridinophane-1,7,14,20-tetrone (14): 15% yield; mp 212 °C (CH_2Cl_2−ether); IR ν_{max} (KBr) cm^{-1} 1710, 1630; ^1H NMR ($CDCl_3$) δ (ppm) 1.99−2.42 (4 H, m), 3.56−3.69 (4 H, m), 4.23−4.51 (4 H, m), 4.82 (2 H, m), 4.85 (2 H, m), 7.23−7.44 (10 H, m), 7.87−8.16 (6 H, m); ^{13}C NMR ($CDCl_3$) δ (ppm) 24.57 (t), 25.14 (t), 26.46 (t), 42.53 (t), 42.75 (t), 43.88 (t), 46.07 (t), 48.11 (t), 51.94 (t), 60.77 (t), 62.75 (t), 66.68 (t), 123.30 (d), 123.51 (d), 124.53 (d), 127.38 (d), 127.60 (d), 127.78 (d), 127.96 (d), 128.37 (d), 128.56 (d), 128.72 (d), 136.28 (d), 136.63 (s), 136.78 (s), 137.22 (s), 138.01 (d), 138.36 (d), 147.24 (s), 148.23 (s), 152.12 (s), 152.73 (s), 163.97 (s), 164.41 (s), 168.22 (s), 169.51 (s); MS *m*/*z* 592 (M^+, 24), 501. Anal. Calcd for $C_{34}H_{32}N_4O_6$: C, 68.92; H, 5.41; N, 9.46. Found: C, 69.0; H, 5.6; N, 9.4.

6,8-Dioxa-2,12-diaza[13](2,6)pyridinophane-1,7,13-trione (15). Method A. A stirred solution of **7** (1.8 g, 6.4 mmol), triethylbenzylammonium chloride (20 mg), and 1,3-dibromopropane (3.88 g, 19.2 mmol) in dry acetonitrile (40 mL) containing a suspension of K_2CO_3 (anhydrous, 5.3 g, 0.038 mol) was refluxed at 90−100 °C for 24 h. After completion of the reaction, the solid suspension was filtered off, the residue was washed with ethyl acetate, the combined filtrate was distilled off, and the residue was chromatographed to isolate **15** (23%).

Method B. A solution of **7** (1.0 g, 3.56 mmol) and diethyl carbonate (0.42 g, 3.56 mmol) in DMF (25 mL) containing a suspension of NaH was stirred at room temperature. After completion of the reaction (TLC, 24 h), the solid suspension was filtered off. The filtrate was concentrated in vacuum and was chromatographed to isolate **15** (33%): mp 250 °C (EtOH); IR ν_{max} (KBr) cm^{-1} 3400, 1745, 1655; ^1H NMR ($CDCl_3$) δ (ppm) 2.05 (4 H, quint, J = 5 Hz), 3.78 (4 H, q, J = 5 Hz, collapses to triplet on D_2O exchange), 4.45 (4 H, t, J = 5 Hz), 7.99−8.40 (3 H, m), 8.59 (2 H, br, exchanges with D_2O); ^{13}C NMR ($CDCl_3$) δ (ppm) 27.80 (t), 39.20 (t), 69.79 (t), 125.03 (d), 138.88 (d), 148.90 (s), 153.56 (s), 163.02 (s); MS *m*/*z* 307 (M^+, 77), 279 (M^+ − CO, 100). Anal. Calcd for $C_{14}H_{17}N_3O_5$: C,53.86; H, 5.55; N, 11.53. Found: C, 53.9; H, 5.6; N, 11.5.

5,7-Dioxa-2,10-*N*,*N*-dimethyldiaza[11](2,6)pyridinophane-1,11-dione (17). To the solution of **5** (1 g, 3.5 mmol) in dichloromethane were added saturated NaOH solution (10 mL) and TBA HSO_4 (10 mg), and the reaction mixture was stirred overnight. The organic layer was separated and dried over Na_2SO_4, and solvent was removed under vacuum. The crude mixture was chromatographed over silica gel to isolate **17** (3%): mp 157 °C (EtOH); IR ν_{max} (KBr) cm^{-1} 1625; ^1H NMR ($CDCl_3$) δ (ppm) 2.92−3.29 (8 H, m), 3.59−3.68 (2 H, m), 3.98−4.15 (2 H, m), 4.43−4.70 (4 H, m), 7.72−8.03 (3 H, m); ^{13}C NMR ($CDCl_3$) δ (ppm) 36.16 (q) and 40.84 (q), 48.92 (t), 51.04 (t), 63.59 (t), 66.34 (t), 94.23 (t), 124.44 (d), 125.87 (d), 138.44 (d), 150.71 (s), 152.14 (s), 167.19 (s), 168.94 (s); MS *m*/*z* 293 (M^+, 92). Anal. Calcd for $C_{14}H_{19}N_3O_2$: C, 57.33; H, 6.48; N, 14.33. Found: C, 57.2; H, 6.2; N, 14.7.

Crystal Structure Determinations. Data for all the crystals were measured at room temperature using a Seifert XRD 3000S diffractometer with graphite-monochromatized Cu Kα radiation to a maximum θ value of 65°. Two standard reflections were measured after every 100 reflections. Cell constants were refined using the LSCUCRE[14] program with 43, 45, and 52 reflections for crystals **9**, **11**, and **14**, respectively. The data were corrected for Lorentz and polarization effects but not for absorption. The structures were solved by direct methods with SIR92.[15] All of the known hydrogen atoms were refined anisotropically using full-matrix least-squares methods.[16,17] Hydrogen atoms were attached geometrically, and they were not refined. The author has deposited atomic coordinates for **9**, **11**, and **14** with the Cambridge Crystallographic Data Centre. The coordinates can be obtained, on request, from the Director, Cambridge Crystallographic Data Centre, 12 Union Road, Cambridge, CB2 1EZ, UK.

Extraction Measurements. An aqueous solution (2 mL) of metal picrate (0.01 mol L^{-1}) and a chloroform solution (2 mL) of the macrocycle (0.01 mol L^{-1}) were shaken in a cylindrical tube closed with a septum for 5 min and kept at 27 ± 1 °C for 3−4 h. An aliquot of chloroform layer (1 mL) was withdrawn with a syringe and diluted with acetonitrile to 10 mL. The UV absorption of this solution was measured against a blank solution at 374 nm. Extraction of metal picrates has been calculated as the percentage of metal picrate extracted in chloroform layer, and the values are the mean of three independent measurements, which were within ±2% error (Table 1).

Transport Measurements. Transport experiments were carried out in a cylindrical glass cell consisting of outer and inner jackets by using (i) metal picrate (0.01 mol L^{-1}) in water (3 mL) in the inner phase; (ii) water (10 mL) in the outer phase; (iii) ligand (10 mmol L^{-1}) in the chloroform layer (15 mL) with stirring (150 ± 5 rpm) at 27 ± 0.05 °C. After the mixture was stirred for 8 h, the concentrations of the picrates transported in the aqueous receiving phase were determined from the UV absorptions at 355 nm. Each value is a mean of three experiments that are consistent within ±10% (Table 2). Before the transport rates were determined, blank experiments were performed in the absence of the carrier macrocycle in the chloroform layer to check the leakage of metal picrates. Only a significant leakage was observed in case of Pb^{2+}, and so, the results of Pb^{2+} transport are not included in Table 2.

Acknowledgment. We thank DST for a research grant (SP/SI/G23/93) and RSIC, Chandigarh, for elemental analysis. G.H. thanks the Ministry of Science and Education, Spain, for a postdoctoral fellowship.

JO960859S

(14) Appleman, D. E. LSUCRE; US Geological Survey, Washington, DC, 1995, unpublished results.

(15) Altomare, A.; Cascarano, G.; Giacovazzo, C.; Guagliardi, A.; Burla, M. C.; Polidori, G.; Camali, M. SIR92, Program for Crystal Structure solution, University of Bari, Italy, 1992.

(16) Stewart, J. M., Ed. *The X-ray System of Crystallographic Programs*; Computer Science Centre: University of Maryland, College Park, MD, 1980.

(17) Hall, S. R., Flack, H. D., Stewart, J. M., Eds. *XTAL 3.2 Reference Manual*; University of Western Australia, Geneva, Switzerland, and Maryland, 1992.